Int. J. Electrochem. Sci., 7 **(2012)** 5837 - 5863

International Journal of ELECTROCHEMICAL SCIENCE
www.electrochemsci.org

Electrochemical, ESR and Theoretical Insights into the Free Radical Generation by 1,1'-Hydrocarbylenebisindazoles and Its Evaluation as Potential Bio-Active Compounds

Benjamín Aguilera-Venegas[1], *Claudio Olea-Azar*[1,*], *Vicente J. Arán*[2], *Juan Diego Maya*[3], *Ulrike Kemmerling*[4], *Hernán Speisky*[5], *Fernando Mendizábal*[6]

[1] Departamento de Química Inorgánica y Analítica, Facultad de Ciencias Químicas y Farmacéuticas, Universidad de Chile , Casilla 233, Santiago, Chile
[2] Instituto de Química Médica, Consejo Superior de Investigaciones Científicas, Juan de la Cierva 3, 28006 Madrid, España
[3] Departamento de Farmacología Molecular y Clínica, Facultad de Medicina, Universidad de Chile, Santiago, Chile
[4] Programa de Anatomía y Biología del Desarrollo, ICBM, Facultad de Medicina, Universidad de Chile, Independencia 1027, Santiago, Chile
[5] Laboratory of Antioxidants, Institute of Nutrition and Food Technology, University of Chile, Av. Macul 5540, Santiago, P.O. Box 138-11, Chile
[6] Departamento de Química, Facultad de Ciencias, Universidad de Chile, Casilla 653, Santiago, Chile
[*]E-mail: colea@uchile.cl

Received: 27 May 2012 / *Accepted:* 16 June 2012 / *Published:* 1 July 2012

A comprehensive multidisciplinary study is conducted here in order to assess the electrochemical behavior of a series of 1,1'-hydrocarbylenebisindazoles derivatives and its potential use as anti-*T.cruzi* drugs. At first, we have determined the electrochemical reduction mechanisms of this family by cyclic voltammetry (CV) studies, from which three kind of reduction mechanisms -depending on the substituent at positions 3 and 3'- were established, but sharing a first common step corresponding to the generation of a nitro anion radical, which was corroborated by ESR spectroscopy, showing a comparable hyperfine splitting pattern and a strong influence on the ESR spectral linewidths due to the radical-solvent interactions. Furthermore, in order to give a rational description about the electrochemical and ESR results, open- and closed-shell structures of bisindasoles were subjected to theoretical estimations at different levels of theory. For open-shell structures, the hyperfine splitting patterns were confirmed while for the closed-shell systems case, clear evidence about the electrochemical reactivity -in terms of their frontiers orbitals- were obtained. To conclude, all these compounds were assayed as growth inhibitors against *T.cruzi*, from which some degree of activity was observed for this family, highlighting a compound almost as active as the reference drug. Finally, in order to get some information about the potential action mechanisms involved in the trypanocidal activity, molecular modeling and spin trapping studies were also done.

Keywords: bisnitroindazoles / Carbonyl reduction / free radical / spin trapping / microsomal ROS production.

1. INTRODUCTION

American trypanosomiasis (commonly known as Chagas' disease) is one of the fastest growing diseases in Latin America[1]. The causative agent of this disease is the haemoflagellate protozoan *Trypanosoma cruzi* (*T.cruzi*), which is transmitted in rural areas to humans and other mammals by reduviid bugs such as *Rhodnius prolixus* and *Triatoma infestans*[2]. Currently, this pathology is treated with nitroheterocyclic agents such as nifurtimox (Nfx) and benznidazole (Bnz), controversial because of the variety of undesirable side effects.[3]

It is believed that both drugs act through different action mechanisms,[4] however, a common first step is shared between them: the one-electron reduction of the nitro group to form a nitro anion radical $RNO_2^{\bullet-}$,[3, 5-7] relevant in terms of their biological activities, since the stability of this radical is related to the capacity to induce the formation of reactive oxygen species (ROS) into the parasite,[6, 8, 9] vulnerable to the redox unbalance.[7] Thus, $RNO_2^{\bullet-}$ plays a key role in the biological activity, and the understanding of its behavior is a permanent challenge for nitro-derivatives. Taking this into account, ESR spectroscopy has been one of the most significant tools for analyzing the electronic structure of free radical species, allowing the specific reduction of an active electrochemical moiety[10] and obtaining of relevant information on the electronic structure of free radicals and its structural relaxation upon reduction processes,[11] and especially, because it allows the elucidation of relevant parameters on the ROS production in biological systems.[12-14]

In the search for new alternatives to the obsolete Nfx and Bzn, 5-nitroindazoles have shown interesting tripanocidal properties against *T.crizi*, highlighting the ROS production as a potential action mechanism involved in the trypanocidal activity,[15-18] even when, their mechanisms of action still remain without being clarified and therefore, other potential action mechanisms have had to be explored.[5, 19, 20]

Consequently, exclusive of kinetoplastid parasites, trypanothione reductase (TR) plays a key role in redox-homeostasis, catalyzing the regeneration of trypanothione disulfide ($T[S]_2$) to trypanothione ($T[SH]_2$) (a low molecular-weight thiol able to inactivate free radicals) and responsible for maintaining a reduced environment, essential for the growth and survival of the parasite[21-26]. In addition, $T[S]_2$-TR has shown to have a similar role to glutathione-glutathione reductase (GSSG-GR) system in mammal cells,[22] sharing around a 40% in their sequences.[27] However, the pronounced differences in substrate specificity,[28] have exposed the $T[S]_2$-TR active site as a promissory target for drug design.[22, 29]

Regarding the aforementioned, potential anti-*T.cruzi* drugs have been proposed. In our case, we have focused on improving the trypanocidal activity through chemical modifications on several nitrocompunds in order to increase the ROS production into the parasite.[30-33] However, our latest evidence about the trypanocidal activity of nitroquinoxaline and nitroindazole derivatives would have its origin as the result of a concomitant action mechanism between the ROS production and TR inhibition,[19, 34] which has led us to propose the TR inhibition by nitro compounds, as a feasible action mechanism involved in the tripanocidal activity, a relevant outcome to consider for the design of new trypanocidal drugs.

On the other hand, a new series of bis(nitroindazoles) (figure1) with confirmed antiparasitic activity against *Plasmodium falciparum* has been synthesized.[35] Nevertheless, in spite of having been designed with the purpose of inhibiting the biocrystallization of ferriprotoporphyrin IX (heme) to hemozoin in *P.falciparum*,[36] the presence of electroactive groups (NO_2 and CO) as well as the main structure based on the indazole ring, enable this family as potential anti-*T.cruzi* drugs.

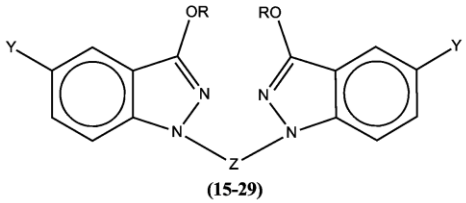

(15-29)

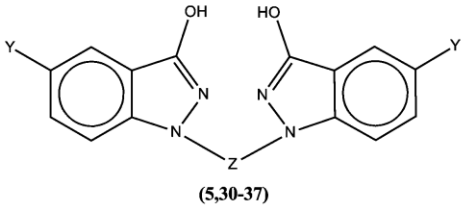

(5,30-37)

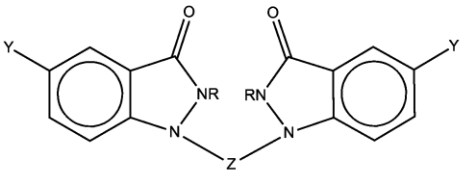

(40-42)

Z	R=Bn Y=NO_2	R=Me Y=NO_2	R=Me Y=H	Y=NO_2	R=Me Y=NO_2
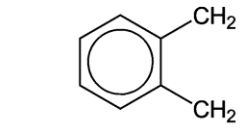	**15**	**20**	**29**	**5**	**40**
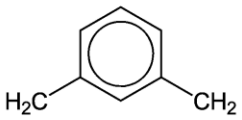	**16**	**21**	—	**30**	**41**
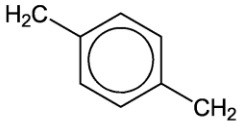	**17**	**22**	—	**31**	**42**
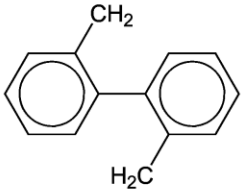	**18**	**23**	—	**32**	—
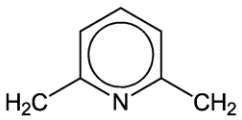	**19**	**24**	—	**33**	—
$[CH_2]_2$	—	**25**	—	**34**	—
$[CH_2]_4$	—	**26**	—	**35**	—
$[CH_2]_5$	—	**27**	—	**36**	—
$[CH_2]_6$	—	**28**	—	**37**	—

Figure 1. Chemical structures of 1,1'-hydrocarbylenebisindazoles derivatives proposed for this study.

However, knowledge of compounds bearing two or more nitro groups is a constant challenge and its behavior has mainly been evaluated for dinitrobenzenes[37, 38] and some dinitrodibenzodioxins,[39] where the NO_2 groups are directly linked to the main ring. Additionally, even when its behavior is strongly dependent on the structural separation of both nitro groups,[40] dinitrocompounds such as some terthiopheno and bis(triarylamine) derivatives containing a determinate moiety as connector, [41, 42] are far less studied than nitroaromatic compounds.

Thus, in this paper we describe a comprehensive study of a new family of bis(nitroindazoles) containing a hydrocarbylene moiety as connector between the two indazole rings (figure 1). We report details of the reduction mechanisms of this family in aprotic solvent as well as an extensive chemical

characterization of the free radicals formed and its rationalization through theoretical calculations. The *in vitro* anti-parasitic activity of these compounds was carried out by means of MTT assays, and finally, in order to get information about the potential action mechanisms that can participate into the trypanocidal action, spin-trapping and molecular modeling studies were also done.

2. EXPERIMENTAL

2.1. Reagents

The absolutely pure 1,1'-hydrocarbylenebisindazoles (figure 1) were provided to us by Dr. V. Aran, which were synthesized according to protocols described before.[35] Dimethyl sulfoxide (DMSO - spectroscopy grade) and tetrabutylammonium perchlorate (TBAP) were supplied from Fluka.

2.2. Cyclic voltammetry

Cyclic voltammetry (CV) was carried out using a Metrohm 693 VA instrument with a 694 VA Stand convertor and a 693 VA Processor in DMSO (*ca.* 1.0×10^{-3} M) under a nitrogen atmosphere at room temperature with TBAP (*ca.* 0.1 M), using a three-electrode cell. A hanging drop mercury electrode (HDME) was used as the working electrode, a platinum wire as the auxiliary electrode, and saturated calomel (SCE) as the reference electrode. For compound **41**, the number of transferred electron for the irreversible wave was calculated by using the equation $i_{pc} = (2.99\text{x}10^5)n(\alpha_{na})^{1/2}AC_oD_o^{1/2}v^{1/2}$,[43] where A is electrode area (in cm^2), D_o is the diffusion coefficient; v is the sweep rate and α_{na} is the charge-transfer coefficient.

2.3. Electron spin resonance spectroscopy

2.3.1. Electrochemical behavior:

ESR spectra were recorded in the X band (9.85 GHz) using a Bruker ECS 106 spectrometer with a rectangular cavity and 50 kHz field modulation. The hyperfine splitting constants were estimated to be accurate within 0.05 G. The bis(nitroindazole) radicals were generated by electrolytic reduction *in situ* at room temperature under the same conditions as for the electrochemical case. ESR spectra of the anion radicals were obtained from the electrolysis solution. The ESR spectra were simulated using the program WINEPR Simphonia 1.25 and ROKI[44] package software. The simulation of the spectra were made using the hyperfine coupling constants (hfcc) obtained experimentally, modifying the line width, modulation amplitude and Lorentzian/Gaussian component in the shape of line, until the resulting spectra reaches the greatest similarity with the experimental ones.

2.3.2. Biological ESR measurement:

Spin trapping assays[6] were done using a microsomal fraction (6-8 mg protein/mL) obtained from *T.cruzi*, in a reaction medium containing 1 mM NADPH, 100 mM DMPO, in 20 mM phosphate buffer, pH 7.4. The experiments were done after 15 min of incubation at 28 °C with the respective bis(nitroindazole) in *T.cruzi* microsomal fraction, NADPH and DMPO under aerobic conditions. (8 $x10^7$ cells correspond to 1 mg protein or 12 mg of fresh weight).

2.4. Biological assays

2.4.1. Cytotoxicity in macrophages (RAW 264.7) and T.cruzi-trypomastigotes:

Cytotoxicity assays were performed by using the MTT reduction method as described previously.[45] Briefly, $5x10^5$ RAW 264.7 cells/mL were incubated with compound **24** at different drug concentrations in RPMI 1640 culture medium (5% bovine fetal serum) at 37°C in a flat-bottom 96-well plate during 18 h, then, the culture medium was replaced with 100 µL of unsupplemented phenol red free-RPMI. For the experiments with trypomastigotes, 10^7 trypomastigotes Y strain were incubated in unsupplemented phenol red free-RPMI at 37°C for 24 h. 100 µL of the parasite suspension was extracted and incubated with each compound at fixed concentration (100µM) in a flat-bottom 96-well plate. For both experiments, MTT was added at a final concentration of 0.5 mg/mL incubated at 37°C for 4 h, and then solubilized with 10% sodium dodecyl sulfate (0.1 mM in HCl) and incubated overnight. Formazan formation was measured at 570 nm with the reference wavelength at 690 nm in a multiwell reader Asys Expert Plus©,Austria.

2.4.2. Nephelometry in T.cruzi-epimastigotes:

T.cruzi epimastigotes Y strain, from our own collection were grown at 28 °C in Diamond's monophasic medium, as reported earlier [46] but replacing blood by 4 µM hemin. Fetal calf serum was added to a final concentration of 4%. Compound **24** (dissolved in DMSO) was added to a suspension of 3×10^6 epimastigotes/mL (reaching a DMSO final concentration of 1% in reaction mixture). Parasite growth was followed by nephelometry for 10 days. From the epimastigote exponential growth curve, the culture growth constant (*k*) were calculated, which corresponds to the slope resulting from plotting the natural logarithm (Ln) of nephelometric measurement vs. time. IC_{k50} is the drug concentration needed to reduce the *k* value in 50% and it was calculated by lineal regression analysis from the *k* values at the concentrations used. Reported values are mean of at least three independent experiments.

2.5. Theoretical Calculations

The 1,1'-hydrocarbylenebisindazoles were full optimized to different level theory to reach the best degree of exactitude and precision in the calculations and so can realize a fine-prediction of the hyperfine splitting pattern. For obtain the best structure and find the minimum energy structures with

the highest abundance conformer population in the gas phase a conformational search was performed using molecular mechanics methods (MMFF) as implemented in Spartan'04. Then, the best conformer was optimized with AM1 semiempirical method.[47-50] The final geometry optimization for each selected conformer was performed by means of methods based on the density functional theory (DFT), particularly suitable for the analysis of magnetic properties for open-shell species,[51] and implemented in the GAUSSIAN'09.[52] If no additional information, single point calculations for neutral or free radical structures were performed with the Becke's three parameters exact exchange functional (B3)[53] combined with gradient corrected correlation functional of Lee-Yang-Parr (LYP)[54] of DFT method (U)B3LYP/6-31G(d,p) in vacuum and also with the Polarizable Continuum Model (PCM) solvent methodology.[55, 56] Molecular orbitals were analyzed by using the programs AOMix [57, 58] and GaussSum2.2.[59]

2.6. Molecular Modeling

2.6.1. Autodock Methodologies:

Autodock3.0.5[60] with Lamarckian Genetic Algorithm (LGA) was used to generate the starting complexes. The parameters used for the global search was an initial population of 150 individuals, with a maximal number of energy evaluations of 15,000,000 and a maximal number of generations of 50,000 as end criterion. An elitism of 1 was used and a probability of mutation and crossing-over of 0.02 and 0.08 respectively. From the best solutions obtained according to these parameters, some of them defined by the user as the best probabilities in our case 0.06 were further refined by a local search method such as pseudo Solis and Wets 'PSW'. The following procedure was employed on the TR docking simulations: 200 runs were done for each case. At the end of each run, the solutions were separated into clusters according to their lowest RMSD and the best score value based on a free empiric energy function. Cluster solutions whose average score was not over 1 kcal mol^{-1} with respect to the best energy obtained from the respective solution were selected and analyzed in terms of their docking energies.

2.6.2 Modeling in Trypanothione Reductase:

Bisindazole derivatives were full optimized as aforementioned with Gaussian09 using the hybrid B3LYP, using electrostatic charges type at the single point calculations. The trypanothione reductase (TR) model (based in the crystallographic structure) was downloaded from Protein Data Bank (PDB ID: 1AOG)[61]. Refinement and assignation of hydrogens (to pH=7.4) was realized with YASARA. AMBER charges were assigned to TR through PDB2PQR.[62, 63] *Autodock* defines the conformational space implementing grids all over the space of the possible solutions. With the aim of testing the ability of *Autodock* to converge into solutions that are inside the TR model; herein, we have defined a grid of 126 points per grid point in the coordinates X, Y and Z with 0.28 Å of spacing between them, in such way that all around the catalytic site is covered.

3. RESULTS AND DISCUSSION

3.1. Cyclic voltammetry - Electrochemical Behavior

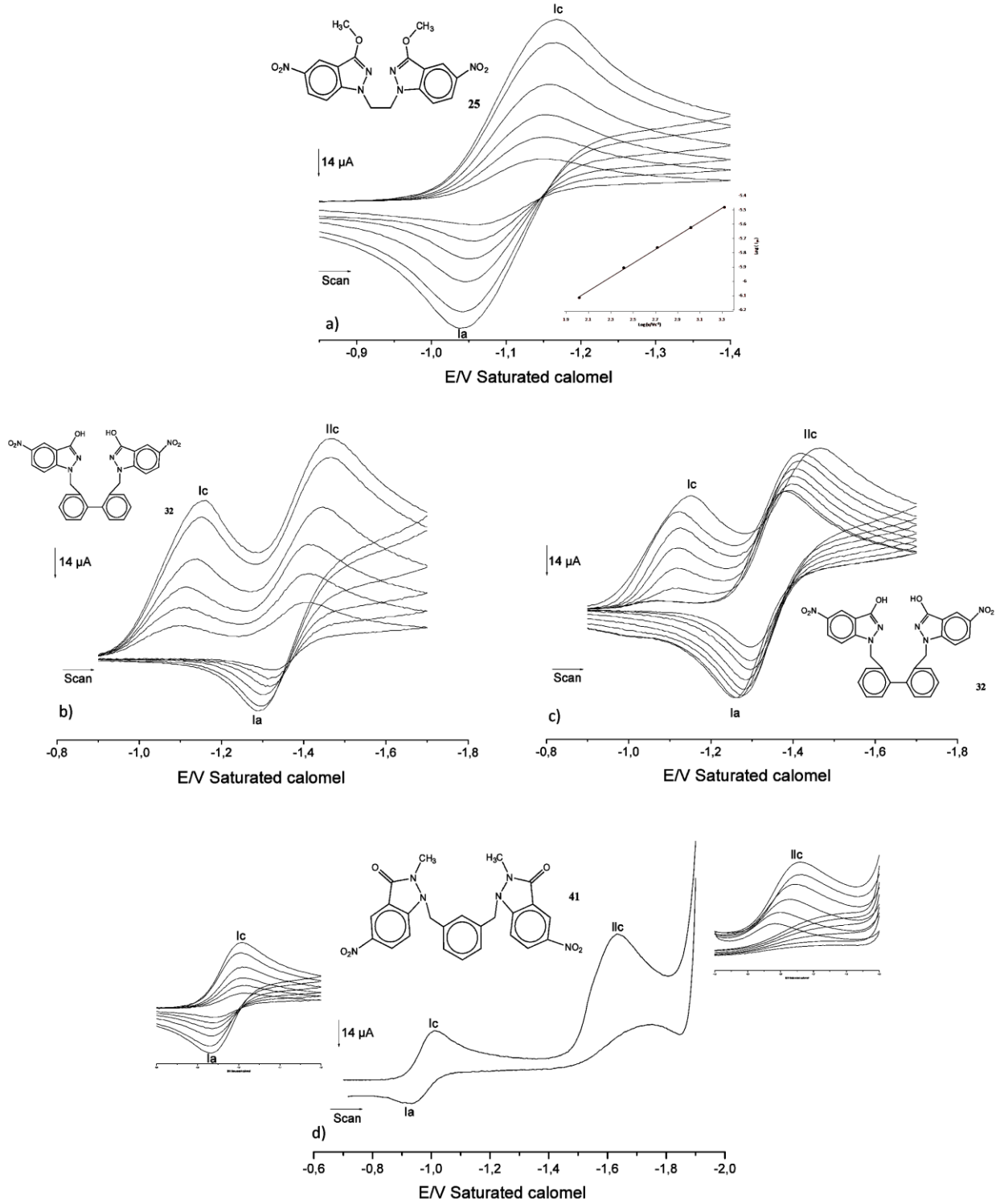

Figure 2. Cyclic voltammograms of 1,1'-hydrocarbylenebisindazoles at 1mM of the derivative in aprotic medium (DMSO+0.1M TBAP) at different sweep rates (100 to 2000 mVs−1) for derivatives a) **25** (3-alkoxy), b) **32** (3-hydroxy), c) **32** (when NaOH(0.1M) is applied from 0 to 1mM) and d) **41** (3-one derivatives).

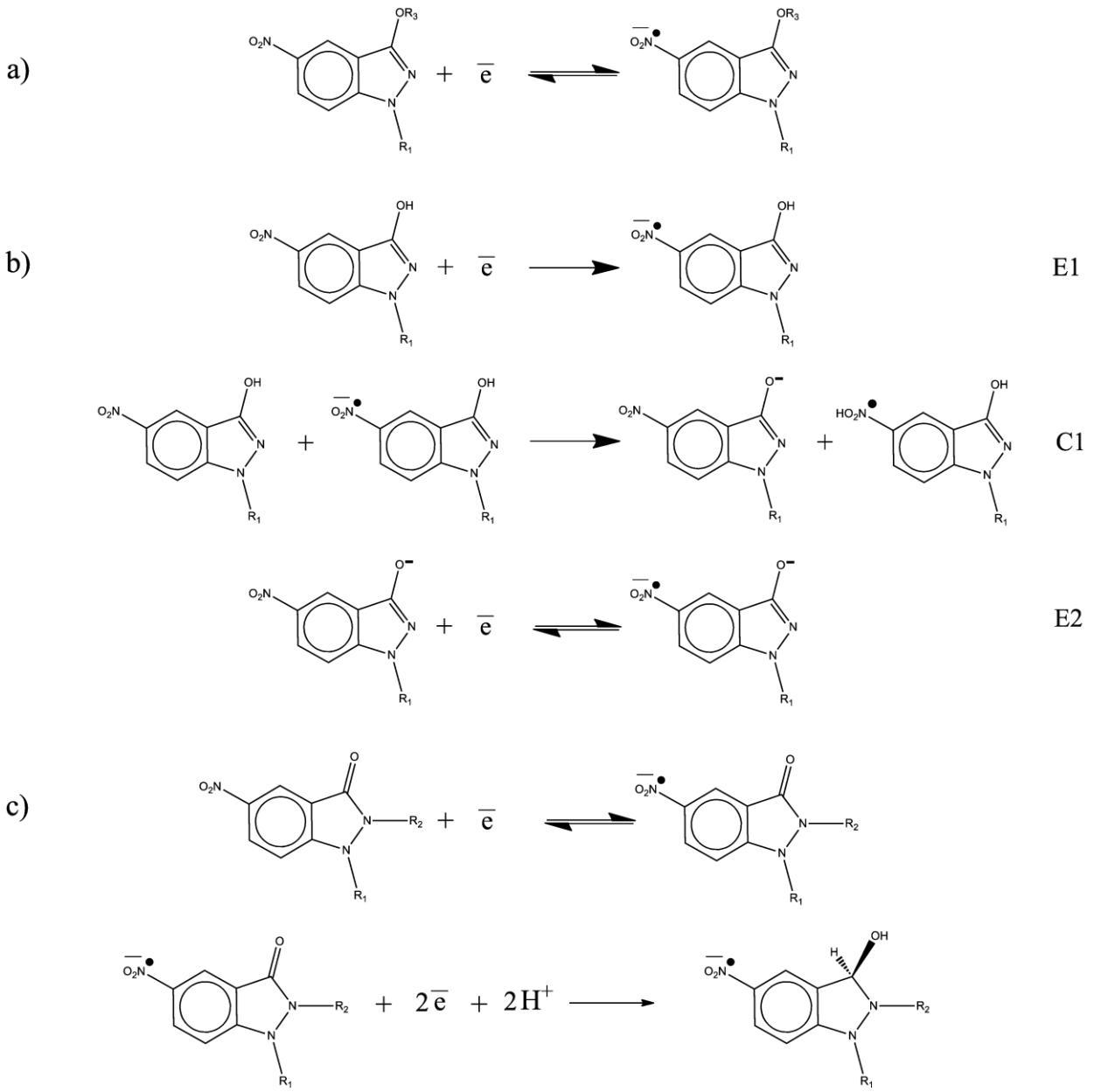

Figure 3. Electrochemical reduction mechanisms for 1,1'- hydrocarbylenebisindazoles: a) 3-alkoxy, b) 3-hydroxy and c) 3-one derivatives.

The electrochemical study in non-aqueous medium (DMSO) showed three reduction mechanisms for this bisindazole family as follows:

In order to achieve the best experimental conditions that ensure the nitro-anion radical stability, an aprotic medium formed by DMSO and TBAP as supporting electrolyte was used. Under these conditions, 3-benzyloxy (15-19) and 3-methoxy (20-28) derivatives displayed a comparable voltammetric behaviour showing only a well-defined quasi-reversible reduction wave. For instance, figure 2a shows the cyclic voltammogram for compound **25**, where a mono-electron reduction (peak Ic/Ia, around −1.1 V) corresponding to the generation of the nitro-anion radical $RNO_2^{\bullet-}$ is evidenced. Then, in absence of conjugation between the indazole rings, the formation of the corresponding

bis(anion radical) would not be stabilized by resonant effects[64] (increasing its reduction potential) and therefore, the consequent reduction of the second nitro group would probably not be observed within the allowed range in the cyclic voltammetry experiments. However, as we will show in the theoretical and ESR sections, this outcome will be confirmed.

On the other hand, the dependence of the cathodic peak current with the sweep rate shows a linear profile with a slope of 0.483 (graph inset in figure 2a) indicating that the electron transference corresponds to a diffusion controlled process without adsorption interference.

Table 1. Electrochemical parameters in DMSO versus saturated calomel electrode (sweep rate $2Vs^{-1}$)

	Epc(I)/V	Epa(I)/V	Epa(II)/V	Ipa/Ipc	ΔE/V	$E_{1/2}$/V
5	-1.13	-1.41	-1.31	0.18	0.10	-1.36
15	-1.19	-0.97	-	0.56	0.22	-1.08
16	-1.08	-1.01	-	0.70	0.07	-1.04
17	-1.16	-0.95	-	0.70	0.30	-1.10
18	-1.05	-0.97	-	0.59	0.08	-1.02
19	-1.19	-0.98	-	0.68	0.21	-1.08
20	-1.09	-1.00	-	0.63	0.08	-1.05
21	-1.12	-1.05	-	0.65	0.08	-1.09
22	-1.12	-1.03	-	0.58	0.09	-1.07
23	-1.13	-1.04	-	0.58	0.08	-1.08
24	-1.22	-0.98	-	0.56	0.24	-1.10
25	-1.17	-1.04	-	0.70	0.13	-1.11
26	-1.12	-1.03	-	0.73	0.09	-1.07
27	-1.15	-1.07	-	0.56	0.08	-1.11
28	-1.14	-1.06	-	0.42	0.08	-1.10
30	-1.16	-1.44	-1.31	0.23	0.13	-1.38
31	-1.32	-1.66	-1.23	0.19	0.44	-1.45
32	-1.13	-1.38	-1.26	0.27	0.12	-1.32
33	-1.12	-1.40	-1.28	0.28	0.12	-1.34
34	-1.14	-1.40	-1.29	0.25	0.11	-1.34
35	-1.15	-1.46	-1.30	0.24	0.17	-1.38
36	-1.13	-1.40	-1.29	0.32	0.11	-1.34
39	-1.07	-1.00	-	0.71	0.07	-1.04
40	-1.11	-0.94	-	0.64	0.17	-1.02
41	-1.00	-0.93	-1.68	0.69	0.07	-0.97
42	-1.07	-0.99	-	0.74	0.09	-1.03

For compounds containing a labile hydrogen (5, 30-37), two reduction waves are distinguished (figure 2b); one cathodic peak (Ic) corresponding to the nitro-anion radical $RNO_2^{\bullet -}$ generation (E1, figure 3b), and then, the wave IIc corresponding to the electroreduction of the anion RNO_2^- (E2, figure

3b) through a self-protonation reaction (C1, figure 3b). This self-protonation process corresponds to an acid–base equilibrium in aprotic solvent, typical behaviour displayed by nitro-compounds with acidic moieties in their structure.[65-67]Additionally, the intensity ratio ipa/ipc (calculated by the Nicholson and Shain equations) is increased when increasing the sweep speed, which indicates a charge transfer process coupled to a reversible chemical process.[68-70] Then, self-protonation phenomenon was corroborated by means of the application of increasing amounts of NaOH (0.1 M) (figure 2c) until obtain only the quasi-reversible wave corresponding to the reduction of the nitro anion to its radical form like dianion radical (E3, figure 3b) which reaches a higher degree of reversibility (deducted from the relation ipa/ipc, whose value is closer to 1 than for the protonated specie), probably because the self-protonation step is excluded when the reduction is going from the deprotonated molecule. Correspondingly, the slight variations in the reduction potentials (IIc) would correspond to a decrease of the capacity to accept electrons, likely due to the negative charge of the deprotonated initial specie.[18]

Bis(indazolin-3-one) derivatives (40-42) showed a similar voltammetric behavior, displaying the aforementioned quasi-reversible wave corresponding to the reduction of one of the nitroindazole rings (around 1.0 V). However, for compound 41 a new irreversible wave toward more negative potentials was observed (figure 2d, wave IIc), which would correspond to the reduction of the -CO- group through a two electron transfer process as described previously for some carbonyl derivatives,[71, 72] and whose first confirmation is obtained when we applied the equation for completely irreversible waves,[43] where an n~2 value is obtained for this electronic transfer. (See theoretical section for more details about this assignation) Finally, compound 29 (without -NO_2 group) showed no electrochemical response in the range of sweep potential used. All electrochemical mechanisms and parameters are summarized in figure 3 and table 1 respectively.

3.2. ESR spectroscopy - The hyperfine splitting

Free radical generation for 1,1'- hydrocarbylenebisindazoles (1 mM) in DMSO was done through electrolysis *in situ* by applying the reduction potential Epc(I) (corresponding to the nitro anion radical generation) obtained from cyclic voltammetry experiments. The interpretation of the ESR spectra was made through a simulation process that confirms the stability of the radicals due to the delocalization of the unpaired electron, condition that allows us to make a correct distribution of the magnitudes of the hyperfine coupling constants (hfcc) and proposing a hyperfine splitting pattern for this family of radicals.

All free radicals showed comparable and well-resolved spectra. In general terms, the ESR spectra were consistent with a hyperfine splitting pattern composed by two triplets of nitrogen; the first one, assigned to the nitrogen from nitro group with a large hfcc, and the second, corresponding to the nitrogens N-1 and/or N-2 (in function of the substituent in 3 or 3' and the hydrocarbylene moiety) besides six doublets assigned to the hydrogens H-4, -6 and -7, whose clear analogy with mono-nitroindazoles[18] (in terms of number and the shapes of lines from the ESR spectrum as well as in the exhibited splitting patterns) suggests clearly the formation of a single $RNO_2^{\bullet-}$ as product of the

electroreduction at the potential applied. Thus, according to the Robin and Day classification,[73] these bis(nitroindazole) free radicals will have a mixed valence behavior of class II as described for some dinitrobenzenes.[38]

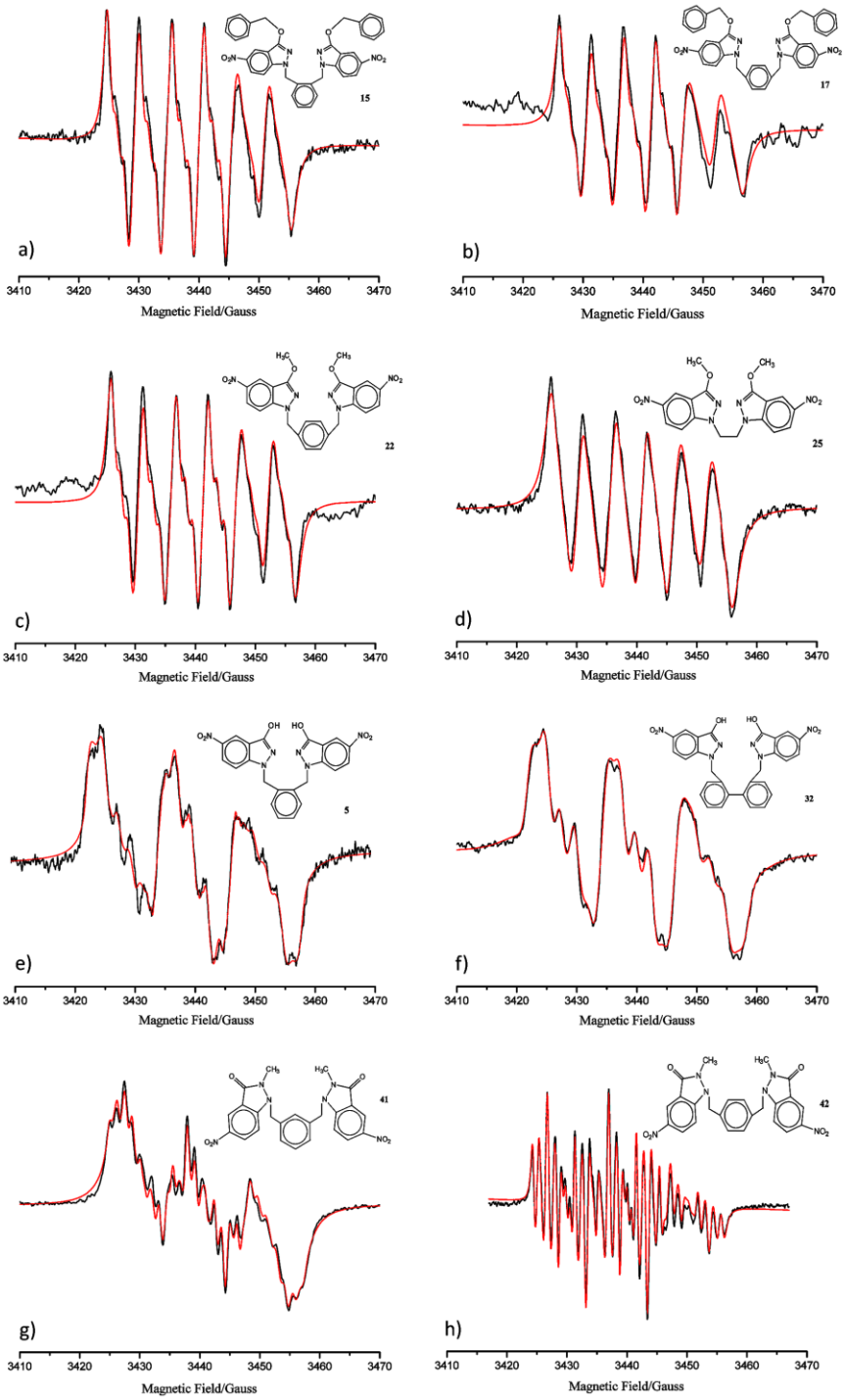

Figure 4. Experimental(black) and simulated(red) ESR spectra of 1,1'- hydrocarbylenebisindazoles (1 mM) free radicals in DMSO generated through electrolysis *in situ* by applying the reduction potential Epc(I) from cyclic voltammetry experiments for compounds a) **15**, b) **17**, c) **22**, d) **25**, e) **5**, f) **32**, g), **41** and h) **42**. Spectrometer conditions: microwave frequency, 9.68 GHz; microwave power, 20 mW; modulation amplitude, 0.20 G; time constant, 81.92 mS.

On the other hand, the experimental ESR spectra showed a remarkable anisotropy in the high field, probably due to the radical-solvent interactions, causing anisotropy in the *g* and hyperfine tensors and producing linewidths alterations into the ESR spectra. However, this drawback in the spectral simulation was solved by using the ROKI[44] simulation software, which allowed us to include the solute-solvent phenomena into the simulations by means of the theory of linewidths in electron spin resonance of Freed and Fraenkel[11, 74]. Thus, an accurate mapping of the magnitude of the hyperfine coupling constants was obtained, allowing a detailed description of the electronic structure of these free radicals besides an excellent agreement between the experimental and simulated spectra. All spectroscopic parameters for simulations are found summarized in the table 2.

Table 2. Experimental hyperfine coupling constants and simulations parameters for 1,1'-hydrocarbylenbisindazole nitro anion radical.[a]

	g	$N(NO_2)$	N-1	N-2	H-4	H-6	H-7	Ha	Hb	LW	β	γ
5	2.0084	11.169	1.716	0.548	4.809	1.299	0.800	0.500	-	0.998	0.169	0.930
15	2.0084	10.846	1.256	-	5.301	0.565	-	-	-	0.783	0.178	0.210
16	2.0079	10.472	-	-	5.153	1.593	-	-	-	2.102	0.178	0.465
17	2.0075	10.755	1.248	-	5.250	0.483	-	-	-	0.983	0.225	0.317
18	2.0079	10.881	1.230	-	5.349	1.662	1.662	0.371	0.468	0.354	0.277	0.373
19	2.0098	10.531	1.164	-	5.226	-	-	-	-	-	-	-
20	2.0060	7.4037	1.972	-	5.286	3.736	0.903	0.802	0.443	0.448	0.072	0.349
21	2.0076	10.750	1.146	-	5.169	-	-	-	-	1.788	0.111	0.170
22	2.0076	10.838	1.289	-	5.301	0.481	-	-	-	0.939	0.112	0.155
23	2.0081	10.878	1.245	-	5.268	0.593	0.047	0.002	-	0.832	0.144	0.190
24	2.0077	10.497	1.069	-	5.188	-	-	-	-	1.856	0.226	0.444
25	2.0079	10.717	1.152	-	5.165	-	-	-	-	1.515	0.093	0.142
26	2.0084	10.995	1.258	-	5.283	-	-	-	-	0.762	0.084	0.091
27	2.0080	10.862	1.258	-	5.244	0.864	0.864	0.543	0.321	0.559	0.094	0.135
28	2.0054	10.768	1.267	-	5.340	-	-	-	-	1.173	0.089	0.177
29	-	-	-	-	-	-	-	-	-	-	-	-
30	2.0083	11.957	1.118	-	4.629	2.332	0.708	-	-	1.203	0.250	0.584
31	2.0080	10.436	1.598	0.540	4.524	1.360	0.897	0.613	0.245	1.485	0.209	1.107
32	2.0103	11.739	1.074	-	4.752	2.295	0.706	0.472	-	1.349	0.180	0.738
34	2.0080	10.436	1.598	0.540	4.865	1.609	0.897	0.613	0.245	-	-	-
35	2.0104	11.581	1.176	-	4.552	2.333	0.774	-	-	1.335	0.137	0.894
36	2.0076	11.907	1.095	-	4.760	2.347	-	-	-	1.530	0.015	0.714
37	2.0079	10.467	1.384	0.951	4.857	2.512	0.613	0.015	-	0.762	0.372	1.175
40	2.0079	10.458	1.351	-	4.541	2.427	1.015	0.310	0.119	0.391	0.138	0.151
41	2.0077	9.7007	1.427	-	4.444	2.468	1.003	-	-	1.095	0.065	0.707
42	2.0082	10.256	1.426	-	4.555	2.444	1.018	0.208	0.160	0.348	0.121	0.135

[a] Hyperfine coupling constants in Gauss units. LW = linewidth. β and γ are resultants parameter from convergence equation[44]. Ha and Hb are coupling constants corresponding to two hydrogens out of the heterocycle.

Thus, having ensured a proper distribution of the hyperfine couplings, a more detailed analysis of the hyperfine patterns is possible as follows:

As mentioned above, the delocalization of the unpaired electron on these bis(nitroindazoles) would be through one of the nitroindazole rings by resonance effects, however, the number and shape of the lines in the ESR spectra were different (figure 4). For instance, alcoxy derivatives (**15-28**) showed an ESR spectrum of 6 lines, the hydroxy derivatives (**5**, **30-37**) one of 9 lines while the 3-one derivatives (**40-42**), one of 28 lines. Such differences would have its origin in terms of the superposition of spectral lines for the case of the alkoxy derivatives and the incidence of self-protonation process for hydroxy derivatives, and probably, the *-meta* and *-para* substitution of the hydrocarbylene fraction bound to the indazole rings for 3-one derivatives, and they all influenced by radical-solvent interactions, which confirms a clear dependence on the shape of the ESR spectra by the substituent at position 3 (as well as the hydrocarbylene moiety), but less impact on their hyperfine splitting patterns.

In spite of the above, some interesting differences between alcoxy and hydroxy derivatives can be appreciated from their hyperfine coupling constants (table 2). For example, for alkoxy derivatives, the coupling constants of N(NO_2 group) and H-4 is around 10 Gauss and 5 Gauss respectively without apparently coupling to N-2. Nevertheless, for 3-hydroxy derivatives the coupling with N(NO_2) is increased to *ca.* 11 Gauss, H-4 is decreased to *ca.* 4 Gauss and the coupling with N-2 is detected (between 0.5 to 1 Gauss for **5**, **31**, **34** and **37** free radicals). These differences would have its origin in the electron donor/attractor properties of the substituent at position 3, where the nature of the moiety produces inductive effects into the delocalization of the unpaired electron causing slight variations into the magnitudes of the hyperfine coupling constants.

Finally, bis(nitroindazolin-3-one) derivatives (**40-42**) have shown well-resolved ESR spectra (figure 4g and 4h). However, as in the previous cases, the hyperfine coupling constants were similar and therefore, and the observed differences in the linewidths of the ESR spectra would be related to the position (*-o, -m, -p*) of the hydrocarbylene substituent and the dynamics effects given by the radical-solvent interactions. Thus, all bis(nitroindazole) free radicals showed comparable and well-resolved spectra, suggesting an similar behavior for these species. Moreover, the similarity observed with ESR spectra of analogous mono nitroindazoles suggests again the formation of a single nitro anion radical as product of the electroreduction and consequently, a mixed valence behavior of class II for bis(nitroindazole) free radicals. The observed differences in the ESR spectra as well as in their hyperfine coupling constants would be given mainly by dynamics effects and the electron donor/attractor properties of the substituent at position 3.

3.3. Theoretical calculations - Electronic structure of free radicals

In order to rationalize the previous results, we have studied the neutral and radical structures under the environment effects.[55, 75-77] Then, with a view to find the most reliable basis-set to describe the bis(nitroindazole) system, the hfcc for compound **5** were estimated under several theoretical methodologies (functional: B3LYP / PBE0 / PBE / B3PW91 // Basis-set : 6-31G+ / 6-

31G++ / 6-31G++(d,p) / LANL2DZ / LANL2MB / EPR-II / EPR-III / aug-cc-PVDZ) [75, 76, 78, 79] and comparing them with the experimental ones. Theoretical estimations under vacuum conditions were not enough to describe the hyperfine structure, even when, an extensive set of basis-set functions were used, showing a comparable partition of the hyperfine constants between the two indazole rings (table 3 and 4) and coupling constants near to half of the experimental ones, which does not agree with the experimental behavior. However, taking into account the solute-solvent interactions and increasing the convergence criteria into the calculations, the hfcc reached the experimental agreement as is described in figure 5 through spin density plots. These results show that the influence of solvent governs the formation of nitro anion radical and the corresponding delocalization on one of the indazole rings.

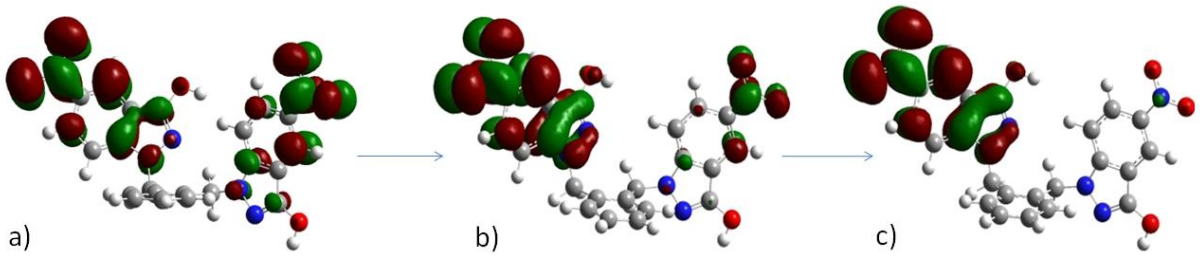

Figure 5. Density spin plot of semi-occupied molecular orbital for molecule **5** free radical under the methodologies: a) UB3LYP/6-31g++(d,p) and vacuum conditions, b) same as a) but including solute-solvent interactions with the PCM solvation model, and c) same as b) but improving the convergence by using the "tight" keyword into the calculations.

Table 3. Theoretical hyperfine coupling constants for compound 5 free radical (nitroindazole moiety experimentally reduced).[a]

Methodology[b]	N(Nitro)	N-2	N-1	H-4	H-6	H-7
UB3LYP/6-31G+	7.665(4.470)	0.029(0.081)	0.284(0.226)	3.971(3.852)	1.524(0.907)	0.965(0.577)
UB3LYP/6-31G++	7.686(4.480)	0.029(0.079)	0.285(0.210)	3.982(3.893)	1.527(0.836)	0.966(0.528)
UB3LYP/6-31G++(d,p)	7.286(4.180)	0.077(0.046)	0.135(0.003)	4.804(4.361)	1.342(0.066)	0.711(0.179)
UB3LYP/ LANL2DZ	5.264(4.211)	0.054(0.105)	0.260(0.231)	3.423(4.083)	1.239(0.821)	0.817(0.507)
UB3LYP/LANL2MB	0.623(0.291)	0.219(0.022)	0.106(0.110)	5.765(5.712)	0.174(0.221)	0.910(1.186)
UB3LYP/EPRII	4.100(2.906)	0.046(0.117)	0.026(0.024)	4.343(4.458)	0.682(0.294)	0.318(0.232)
UB3LYP/EPRIII	4.823(2.532)	0.075(0.023)	0.085(0.002)	4.792(3.468)	0.639(0.244)	0.096(0.036)
UB3LYP/aug-cc-PVDZ	8.289(4.566)	0.093(0.094)	0.186(0.068)	4.301(3.929)	1.169(0.288)	0.653(0.273)
UB3PW91/6-31G+	7.204(4.286)	0.063(0.113)	0.306(0.192)	4.313(4.463)	1.641(0.804)	1.084(0.500)
UB3PW91/6-31G++	7.224(4.348)	0.062(0.109)	0.307(0.254)	4.326(4.296)	1.645(1.030)	1.086(0.680)
UB3PW91/6-31G++(d,p)	6.222(3.228)	0.044(0.131)	0.073(0.228)	5.201(4.851)	1.170(1.040)	0.529(0.686)
UB3PW91/ LANL2DZ	6.152(4.100)	0.077(0.127)	0.285(0.242)	3.753(4.411)	1.366(0.857)	0.938(0.554)
UB3PW91/LANL2MB	0.623(0.292)	0.226(0.041)	0.090(0.105)	5.872(5.880)	0.160(0.230)	0.870(1.188)
UB3PW91/EPRII	3.532(2.097)	0.073(0.126)	0.019(0.033)	4.771(4.477)	0.715(0.452)	0.346(0.154)
UB3PW91/EPRIII	4.285(1.960)	0.037(0.009)	0.015(0.078)	5.063(3.845)	0.700(0.338)	0.253(0.355)
UB3PW91/aug-cc-PVDZ	7.188(3.816)	0.042(0.109)	0.105(0.054)	4.603(4.063)	0.966(0.424)	0.462(0.154)
Experimental[c]	11.16169	0.5489	1.2160	4.8091	1.2998	0.8002

[a] Units = Gauss. NI = nitroindazole

[b] Values in parentheses corresponding to the coupling constants in vacuum conditions.

[c] See table 2

Table 4. Theoretical hyperfine coupling constants for compound 5 free radical (nitroindazole moiety experimentally unreduced).[a]

Methodology[b]	N(Nitro)'	N-2'	N-1'	H-4'	H-6'	H-7'
UB3LYP/6-31G+	4.138(4.156)	0.061(0.100)	0.142(0.173)	1.982(3.296)	0.824(0.799)	0.504(0.482)
UB3LYP/6-31G++	4.112(4.130)	0.061(0.091)	0.141(0.138)	1.967(3.210)	0.818(0.723)	0.499(0.403)
UB3LYP/6-31G++(d,p)	1.745(2.202)	0.034(0.048)	0.054(0.083)	0.993(2.619)	0.378(0.052)	0.231(0.157)
UB3LYP/ LANL2DZ	5.264(3.921)	0.046(0.131)	0.194(0.209)	2.726(3.512)	0.980(0.786)	0.608(0.494)
UB3LYP/LANL2MB	0.580(0.336)	0.173(0.285)	0.005(0.165)	4.200(5.432)	0.144(0.206)	0.330(1.100)
UB3LYP/EPRII	2.412(2.906)	0.014(0.068)	0.048(0.047)	1.667(2.484)	0.526(0.460)	0.216(0.239)
UB3LYP/EPRIII	2.010(2.681)	0.055(0.063)	0.038(0.006)	1.006(3.162)	0.333(0.463)	0.140(0.145)
UB3LYP/aug-cc-PVDZ	1.899(2.832)	0.047(0.047)	0.067(0.077)	0.871(2.164)	0.324(0.430)	0.208(0.236)
UB3PW91/6-31G+	4.293(3.826)	0.071(0.101)	0.168(0.118)	2.372(3.396)	0.973(0.711)	0.621(0.373)
UB3PW91/6-31G++	4.268(4.037)	0.071(0.129)	0.167(0.204)	2.355(3.707)	0.965(0.911)	0.614(0.584)
UB3PW91/6-31G++(d,p)	2.106(2.745)	0.022(0.130)	0.058(0.141)	1.377(3.850)	0.475(0.759)	0.273(0.556)
UB3PW91/ LANL2DZ	5.125(3.850)	0.064(0.149)	0.209(0.192)	2.946(3.778)	1.059(0.775)	0.687(0.487)
UB3PW91/LANL2MB	0.581(0.337)	0.184(0.296)	0.011(0.150)	4.332(5.579)	0.153(0.209)	0.315(1.077)
UB3PW91/EPRII	1.973(1.736)	0.006(0.099)	0.045(0.053)	1.728(3.091)	0.538(0.549)	0.240(0.292)
UB3PW91/EPRIII	1.919(2.681)	0.017(0.068)	0.043(0.070)	1.262(3.139)	0.415(0.690)	0.200(0.317)
UB3PW91/aug-cc-PVDZ	2.483(3.170)	0.029(0.070)	0.078(0.096)	1.248(2.765)	0.412(0.541)	0.245(0.303)

[a] Units = Gauss. NI = nitroindazole
[b] Values in parentheses corresponding to the coupling constants in vacuum conditions

Theoretical estimations under unrestricted formalism have revealed B3LYP and PBE0 as the best hybrids for this kind of molecules. PBE and B3PW91 have shown no correlation whatsoever with the experimental hfcc (table 3, 4 and 5), and therefore, all the following analysis will be based on the hybrids B3LYP and PBE0. With regard to the basis study for hfcc calculations, the basis-set 6-31++G(d,p) and aug-cc-pVDZ were always consistent with the experimental patterns, however with a large computational cost. Pseudo-potential LANL2*XY* basis set does not provide good results in combination with the B3X functional, but it does with the PBE0 functional and also with a notable computational efficiency.

Table 5. Theoretical hyperfine coupling constants for compound 5 free radical (nitroindazole moiety experimentally reduced).[a]

PBE0	N(Nitro)	N-2	N-1	H-4	H-6	H-7
6-31G+	12.136	0.049	0.500	6.744	2.595	1.737
6-31G++	12.135	0.049	0.500	6.740	2.595	1.736
6-31G++(d,p)	9.467	0.087	0.324	6.535	2.256	1.478
LANL2DZ	10.894	0.000	0.459	6.475	2.172	1.472
LANL2MB	0.664	0.269	0.016	6.197	0.055	0.617
EPRII	6.362	0.021	0.158	6.178	1.505	0.934
EPRIII	5.436	0.040	0.027	5.798	0.816	0.312
aug-cc-PVDZ	10.591	0.112	0.410	5.761	1.936	1.315
Experimental[b]	11.161	0.548	1.216	4.809	1.299	0.800

[a] Units = Gauss.
[b] See table 2

Finally, EPR-II and EPR-III basis set have shown a poor performance for hfcc calculations in spite of having been parameterized for it.[80, 81] Thus, the functionals UPBE0/(6-31++G(d,p)/aug-cc-PVDZ/LANL2DZ) and UB3LYP/6-31++G(d,p) have been the most accurate methods for calculations of open-shell structures for bis(nitroindazole) free radicals. Table 6 shows the theoretical hfcc for bis(nitroindazole) through UPBE0/aug-cc-PVDZ methodologies.

Table 6. Theoretical hyperfine coupling constants for 1,1'-hidrocarbilenbisindazole nitro anion radical.[a]

	N(Nitro)	N-1	N-2	H-4	H-6	H-7
5	10.591	0.112	0.410	5.761	1.936	1.315
15	10.661	0.195	0.452	5.902	2.228	1.525
16	10.704	0.165	0.473	5.898	2.231	1.533
19	10.478	0.200	0.447	5.962	2.338	1.553
20	10.499	0.253	0.225	6.064	1.636	1.120
24	10.711	0.609	1.183	5.779	2.261	1.491
25	10.491	0.228	0.316	5.528	1.895	1.183
27	10.892	0.134	0.319	6.093	1.777	1.322
31	10.518	0.152	0.359	5.629	1.787	1.176
33	10.687	0.184	0.442	5.766	2.115	1.406
34	10.465	0.215	0.346	5.585	1.868	1.184
36	10.871	0.205	0.463	5.800	2.208	1.495
37	10.510	0.120	0.282	5.733	1.645	1.069
40	10.413	1.413	0.276	4.829	3.044	1.565
41	10.282	1.497	0.232	4.820	2.909	1.492
42	10.371	1.536	0.272	5.106	2.754	1.512

[a] Methodology: UPBE0/aug-cc-PVDZ/PCM-DMSO.

Returning to the reduction mechanisms, all bis(nitroindazoles) have shown the wave corresponding to the $RNO_2^{\bullet-}$ generation. This fact indicates that despite the presence of two nitro groups (with apparently the same tendency to be reduced), only one nitro group is reduced within the sweep range. Additionally, ESR and theoretical calculations on the open-shell structures support this statement. However, this phenomenon would have its origin in the electronic structure, and therefore, it can be described by molecular orbitals analysis as described below:

In order to assess the influence of the molecular and electronic structure of the bis(nitroindazoles) in the electrochemical reactivity, theoretical evaluations on the closed shell structures were performed and then analyzed through density of states plots. Specifically, with the aim of assessing the structural portions that modulate the electronic structure and its electrochemical reactivity, the entire molecule (compound **5**) was partitioned in five moieties as shown in the inset box in figure 6.

Partial density of states spectra (PDOS, figure 6) suggest that the structural portions that make up the LUMO are mainly given by one of the NO_2 groups, then, in less degree by the hydrocarbylene

moiety and the second NO_2 group, and finally by the indazole rings, which suggest that the second nitro-heterocycle could be partially reduced.

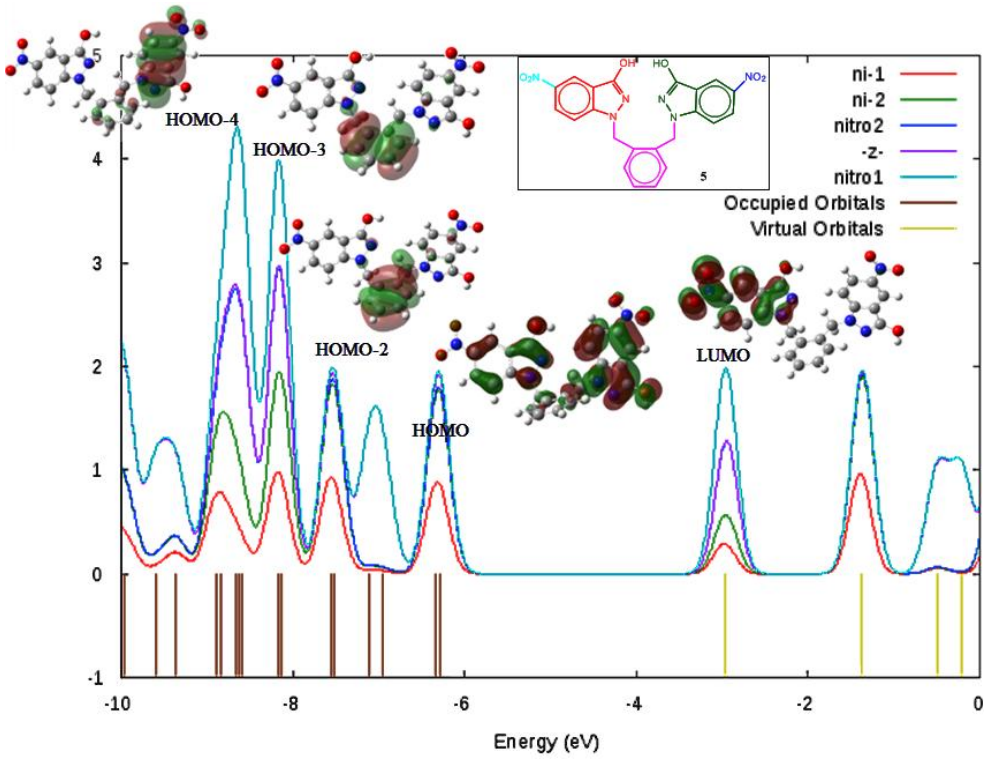

Figure 6. Partial density of states (PDOS) plot for compound **5** under PBE0/aug-cc-PVDZ methodologies.

However, taking into account that the fractions that make up the frontiers HOMOs are given mainly by the hydrocarbylen moiety (HOMO-2 and -3) and by the second nitroindazole (HOMO and HOMO-4), some electronic repulsions between such HOMOs and the SOMO (when the nitro radical generation takes place) are feasible to expect, which would prevent the delocalization of the unpaired electron on these fractions confining the electron delocalization on the nitroindazole moiety with low contribution to the frontiers HOMOs. Thus, -as expected-, the single NO_2 anion radical would by stabilized by resonance effects, but also, the repulsion effects with the frontier HOMOs prevent the partial reduction of the second nitroindazole (LUMO+1), which confirms and explains the electrochemical and spectroscopic behavior observed for this bis(nitroindazole) family.

Under similar arguments, 3-ona derivatives have shown a comparable behavior with some differences. As in the previous case, the LUMO (corresponding to the nitro-reduction) takes place on only one of the nitroindazole rings. However, LUMO+1 (figure 7) instead of being located on the second nitronidazole, it is maintained in the same ring (mainly on CO group) extending itself through the ring by resonance effects but excluding the -NO_2 group probably due to the repulsions with the LUMO (or SOMO -strictly speaking- when the nitro reduction takes place). Molecular orbitals and total density of states (TDOS) plot for compound 41 are shown in figure 7.

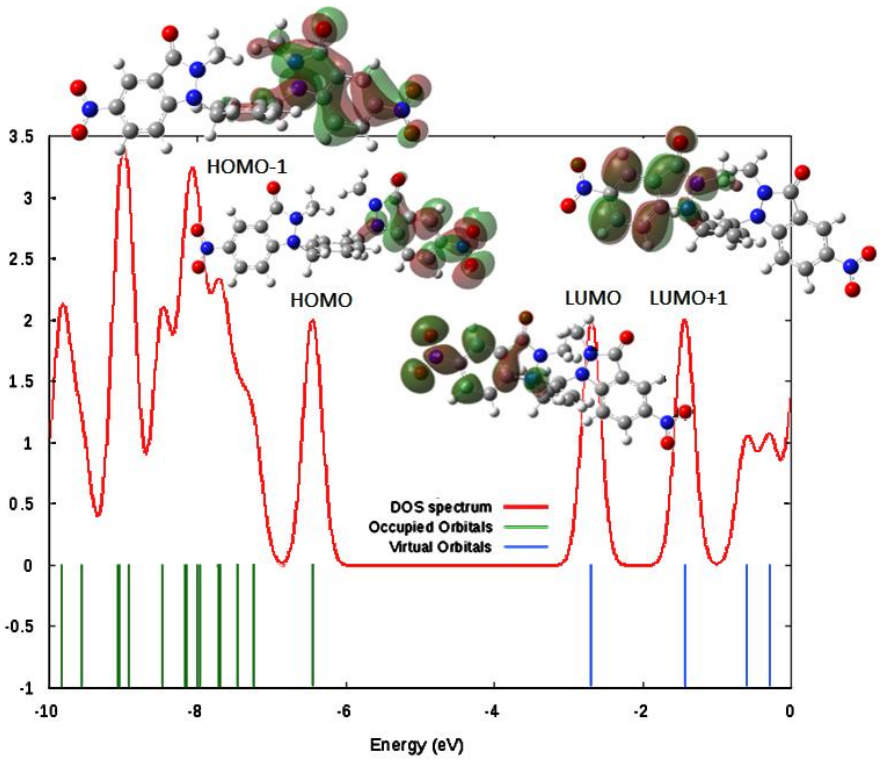

Figure 7. Total density of states (TDOS) plot for compound **41** under PBE0/aug-cc-PVDZ methodologies.

On the other hand, when we explored the electronic structure for compounds **40-42**, no major differences were found that can clarify why the carbonyl reduction for compound **41** can be appreciated in the cyclic voltammetry experiments. However, in terms of the global reactivity for 3-ona derivatives, compound **41** (1,1'-*m*-xylylene substituted) showed a electrophilicity index[82] slightly larger than for –*o* and –*p* derivatives (1.28eV, 1.31eV and 1.29eV for compounds **40**, **41** and **42** respectively) and in correlation with the electrochemical potentials (Epc(I), table 1).

Then, considering this index as a measure of the stabilization energy of the system when it is saturated with electrons coming from the external environment, compound **41** would be better stabilized during the reduction processes, and therefore, their reduction potentials (NO_2 and CO groups) will be lower (easier to reduce) than for compounds **40** and **42**. On these grounds, it is feasible to think that the 1.1'-*m*-xylylene moiety stabilizes the free radical formation, facilitating the reduction processes and allowing the experimental detection of the carbonyl group within the allowable sweep range.

3.4. Biological assays

In order to evaluate the antiparasitic capacity of these compounds, *in vitro* assays in the cellular model of *Trypanosoma cruzi* trypomastigotes (Y strain) were done. The percentage of viable parasites was determined for bis(nitroindazoles) and compared with Nifurtimox (Nfx) as reference drug.

In vitro assays (table 7) reveal that the bis(nitroindazole) derivatives have a certain degree of activity against trypomastigotes of *T.cruzi*. None of them better than Nifurtimox, however, one of them (compound **24**) was almost as active as Nfx.

Table 7. *In vitro* anti-*Tcruzi* (Y strain) activity of 1,1'-hydrocarbylenebisindazoles derivatives

Compound[a]	% viable trypomastigotes[b,c]
5	83.51±0.59
19	87.23±1.23
20	81.35±2.01
24	37.01±0.32
25	94.78±2.43
26	72.56±1.07
27	89.53±1.98
31	83.15±0.67
36	87.64±0.98
38	84.92±1.32
Nfx	23.85±0.28

[a] The remaining compounds could not be tested due to solubility issues.
[b] Values correspond to the percentage of reduction of control trypomastigotes. Compounds tested at 100µM
[c] Results are means of three different experiments with SD less than 10% in all cases

On the other hand, because of the complex culture conditions, the IC_{50} in trypomastigotes could not be calculated. However, for compound **24** the growth inhibition constant (IC_{k50}) in *T.cruzi* epimastigotes as well as in RAW 264.7 macrophages were obtained, yielding values of 51.97µM±0.46µM and 351.07µM±1.57µM respectively, interesting outcome when comparing them with Nfx, ($IC_{50,RAW264.7}$=266.01µM±1.07µM and $IC_{k50,epi\text{-}T.cruzi}$=22,79µM±0,54µM) where despite not show a specific toxicity against *T.cruzi* (IC_{k50} around twice lower than Nfx), the toxicity in macrophages (IC_{50} around 1.3 times better than Nfx) allows us to consider this compound as a viable starting structure for further chemical modifications in order to improve their trypanocidal properties.

Thus, even when only one compound showed an activity comparable to Nifurtimox, bisindazoles have shown some degree of activity against two morphological states of *T.cruzi*, suggesting that these compounds could be an interesting starting family in the search for new trypanocidal drugs.

3.5. Spin trapping studies - Oxidative stress mechanism

As mentioned, it has been exposed that the presence of nitro groups would have direct relation with the trypanocidal properties through the ROS production into the parasite,[34, 83-85] poor in defense mechanisms against the oxidative attack.[86] Thus, in order to investigate the feasibility of these compounds to be metabolized by microsomal enzymes of *T. cruzi* and the potential ROS

production into the parasite, we incubated our derivatives with microsomes of *T.cruzi* in the presence of NADPH and the spin trapping DMPO [6, 17, 85, 87]. Figure 8 shows the ESR spectrum obtained when DMPO was added to the system **24**-*T.cruzi* microsomes as follows:

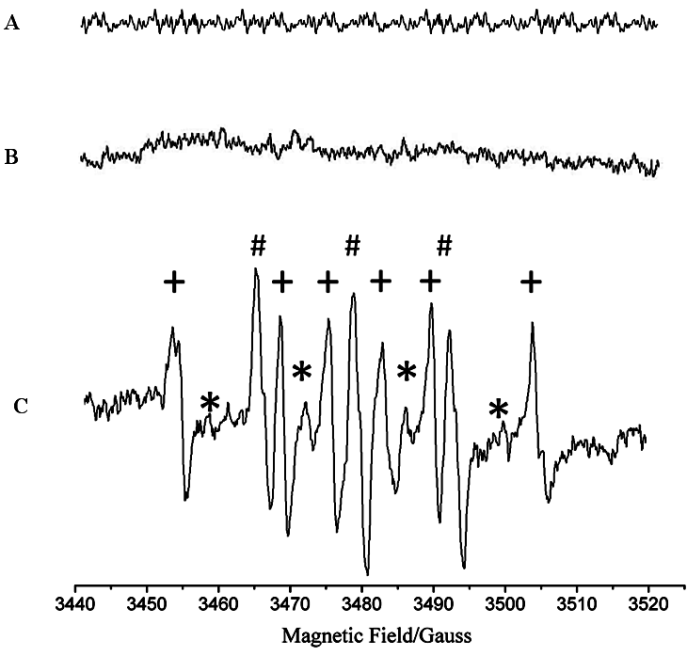

Figure 8. Experimental spectrum for spin-adducts generated in microsomes of *T.cruzi* (Y strain) at 28°C. (A) Control 1: Microsomes in phosphate buffer (20 mM, pH = 7.4), NADPH(1 mM) and DMPO(100 mM). (B) Control 2: Same as control 1, but adding DMSO (10%(v/v)) prior to the addition of DMPO (100 mM). (C) Determination of free radical generating capacity by bisindazoles. Spectra were recorded after prior incubation of the microsomal fraction (8 mg protein/mL), NADPH(1 mM) in phosphate-buffered pH 7.4 and the derivative **24** (2 mM, in DMSO) for 10 min, then, DMPO (100 mM) was added to the system to start the record of the spectrum. In the spectrum are indicated with a symbol (+) the hyperfine pattern corresponding to the spin adduct ·DMPO-CH_3 product of the interaction between the ·OH free radical with the solvent. Additionally, ·DMPO-OH and DMPOX are denoted with the symbols (*) and (#) respectively. The coupling constants for spin-adducts correspond exactly to: aN = 15.4 Gauss and aH = 23.0 Gauss for ·DMPO-CH_3 adduct, aN = 15.2 Gauss and aH = 14.8 Gauss for ·DMPO-OH adduct and aN = 14.6 Gauss for DMPOX.

A thirteen lines spectrum was observed for bis(nitroindazole) derivatives, indicative of the generation of more than one free radical and the consequent formation of the respective spin adducts. The first radical identified corresponds to the trapping of ·OH radical (sign * in figure 8C) directly evidenced from the ESR spectrum by the typical spectrum of four lines with intensities 1:2:2:1 and coupling constants around a_N=15.2G and a_H=14.8G.[88] Moreover, a six lines hyperfine pattern (sign + in figure 8C) was detected and identified as the ·DMPO-CH_3 spin adduct (a_N=15.4G and a_H=23.0G) generated as result of the reaction between ·OH and DMSO with the subsequent trapping by DMPO as follows:[89]

$$\cdot OH + CH_3S(O)CH_3 \rightarrow \cdot CH_3 + HS(O)CH_3$$

$$DMPO + \cdot CH_3 \rightarrow \cdot DMPO\text{-}CH_3$$

On the other hand, the ESR spectra showed a triplet corresponding to the decomposition of DMPO to its twice oxidized form, DMPOX (a_N=14.6G, sign # in figure 8C). However, in the ESR spectrum with DMPO (but without nitro-compound, figure 8A-B) such signals were not observed suggesting that the DMPOX formation (in presence of nitro compound) would be caused by the fast oxidation of ·DMPO-OH radical (already established here) to DMPOX instead of the natural decomposition of DMPO to DMPOX as described by Lawrence et. al.[90] Finally, in order to make sure the trapping patterns, the ESR spectra independently simulated as shown in figure 9.

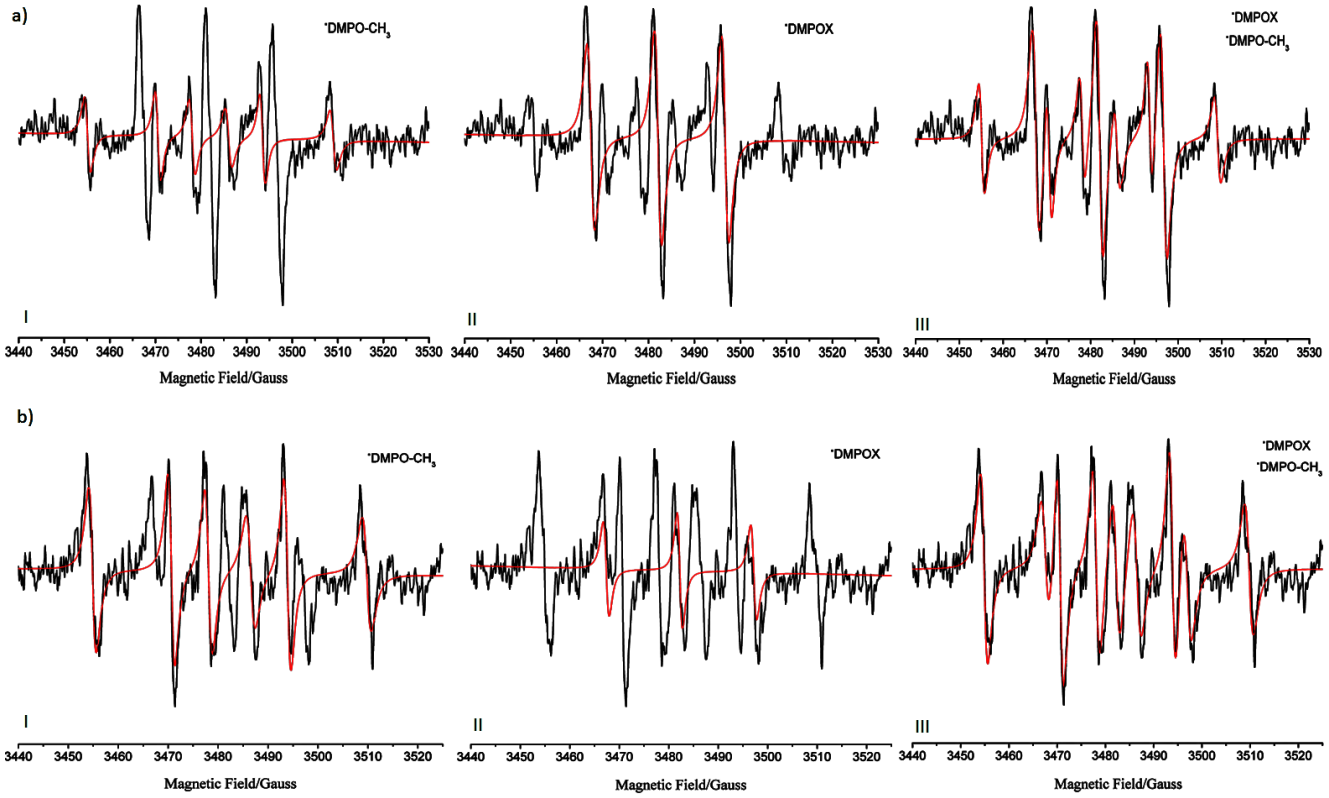

Figure 9. Experimental ESR spectra (black), independent simulations (red, I, II) and overlapping of them (red, III) for the spin-adducts generated in microsomes of *T.cruzi* (Y strain). Recording the spectrum began after to incubate the microsomal fraction (8 mg protein/mL), NADPH (1 mM) in phosphate buffer pH 7.4 and 2 mM (in DMSO) of the compounds (a) **26** as non-positive control and (b) **24** as potential *T.cruzi* drug for 10 min finally adding DMPO (100mM) to start the recording of the spectrum.

From this, the trapping patterns were confirmed, but also, it was found that for compound **24** (as potential anti-*T.cruzi* drug) the trapping signals were increased compared with **26** (as partially non-positive control), which confirms an increase in the ROS production by compound **24**, suggesting that

the ROS production into the parasite will be dependent upon the ability of the nitroderivative of being reduced by the microsomal enzymes (*e.g.* nitroreductases, cyt-p450 and so on) instead of their intrinsic reduction potentials (Epc). Thus, the ROS production by bis(nitroindazoles) has been confirmed, suggesting the oxidative stress as a potential mechanism of action involved in the trypanocidal action.

3.6. Molecular modeling – Inhibition of trypanothione reductase mechanism

In order to evaluate whether this family will present the ability to inhibit TR like some nitroindazoles previously described, molecular modeling studies on the active site of TR were done. The interaction mode for 24-TR complex is shown in figure 10.

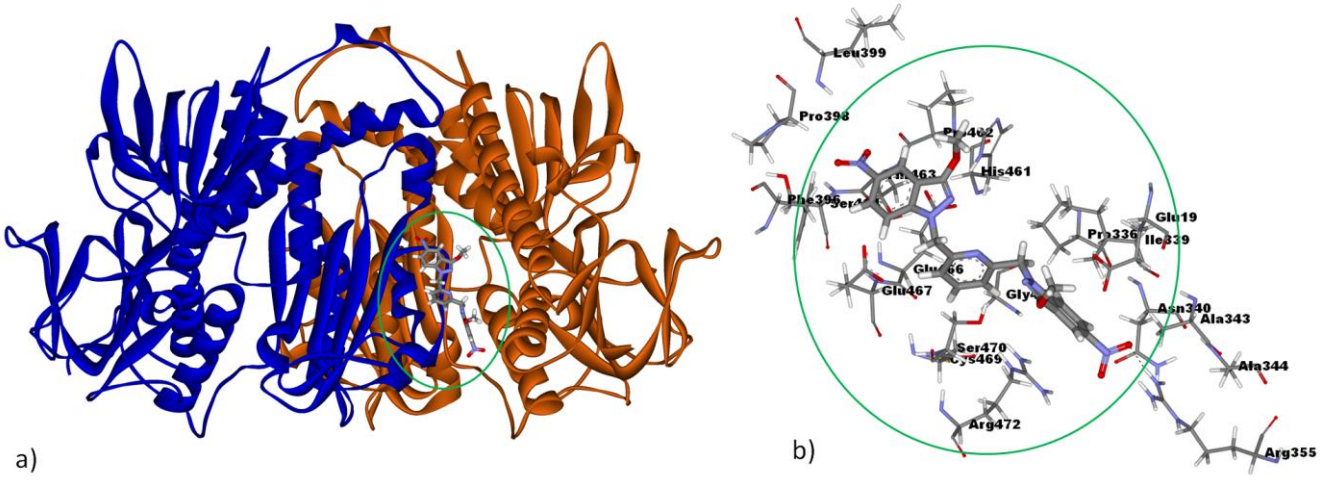

Figure 10. a) General and b) detailed interaction models for 24-TR complex.

Docking results suggest that the conformation adopted by 24 within the TR active site would be mainly governed by hydrophobic contacts, positioning it in a cavity formed by the residues Phe396, Leu399, Met400, Val59, Leu63 and Ala344. Moreover, in the immediate vicinities of the ligand are also found the residues Glu466, Glu467, Lys62, Glu436 and the catalytic residues His461 and Cys58 (relevant for the binding of trypanothione and catalysis) and a potential hydrogen-bond between one of the NO_2 groups with the lateral chain of Arg355, indicative of the participation of electrostatic contacts.

On the other hand, the score associated to this 24-TR complex is *ca.* -12.74 kcal/mol, poorer than the previously described trypanothione-TR complex (-13.68 kcal/mol),[19] which suggests (as an approach) a low partial TR inhibition by bis(nitroindazole). In addition, under a tolerance criterion of RMSD=1Å between potential interacting structures, from the 200 runs specified in the Lamarckian Genetic Algorithm (LGA) calculations, just a few structures were included in the main cluster, showing a wide conformational distribution into the active site, which implies a widespread distribution of the structures into the cavity and a poor convergence towards the active site of TR, suggesting that the specific interaction between the molecule and the enzyme is not enough to inhibit

it. Thus, the interaction between bisindazoles and TR would not be viable, and its inhibition, improbable.

4. CONCLUSIONS

1,1'-hydrocarbylenebisindazoles have shown interesting chemical and biological properties. Electrochemical results indicate that these bis(nitroindazoles) might be electrochemically reduced giving rise to the generation of a stable nitro radical and three types of reduction mechanisms depending on the substituent at positions 3 and 3'. Moreover, ESR results indicate that the hyperfine splitting patterns for the $RNO_2^{\bullet-}$ is composed by the triplets corresponding to N(from NO_2 group), N-1, and/or N-2 besides six doublets corresponding to H-4, -6 and -7, suggesting that the substituents at positions -1 and -3 do not have a major incidences into the splitting patterns, but they do into the linewidths observed in the ESR spectra. Additionally, theoretical calculations confirm the influence of environment on the hyperfine structure of $RNO_2^{\bullet-}$ free radical, besides giving a rational description about the electrochemical reactivity observed for bis(nitroindazoles) in terms of their frontiers orbitals. On the other hand, bisindazoles have exhibited interesting biological properties and some degree of activity against *T.cruzi*, highlighting among them a compound almost as active as the reference drug. Finally, molecular modeling and spin trapping studies suggest that the TR inhibition by bis(indazoles) would not be viable and that the observed trypanocidal activity would be mainly modulated by the ROS production into the parasite. Thus, bisindazoles could be considered as a viable starting family for subsequent chemical modifications in order to improve the anti-*T.cruzi* activity.

ACKNOWLEDGEMENTS
This research was supported by FONDECYT-Chile, ref. 1110029, 1100162, 1090078 and ACT 112 by Spanish Ministry of Science and Innovation, ref. SAF 2009-10399 and by CSIC (Spain)-CONICYT (Chile) collaboration project, ref. 2009CL0011. B. Aguilera-Venegas is grateful to: CONICYT-Doctoral scholarship, ref. 21080766, Support of Thesis, ref. AT-24100009, MECESUP and VAA(University of Chile) for scholarships for research stays. Finally, we thank Antal Rockenbauer for allowing us to use his ESR simulation software.

References

1. C.J. Schofield, J. Jannin, R. Salvatella, *Trends in Parasitology*, 22 (2006) 583-588.
2. W. De Souza, Basic Cell Biology of Trypanosoma cruzi, *Current Pharmaceutical Design, Bentham Science Publishers* Ltd., 2002, pp. 269.
3. J.A. Castro, M.M. deMecca, L.C. Bartel, *Human and Experimental Toxicology*, 25 (2006) 471-479.
4. R. Docampo, S.N.J. Moreno, *Free radicals in Biology*, 4 (1984) 243-288.
5. J.R. Coura, S.L.d. Castro, *Memórias do Instituto Oswaldo Cruz*, 97 (2002) 3-24.
6. C. Olea-Azar, C. Rigol, F. Mendizabal, A. Morello, J.D. Maya, C. Moncada, E. Cabrera, R. di Maio, M. Gonzalez, H. Cerecetto, *Free Radical Research*, 37 (2003) 993-1001.
7. J.A. Urbina, R. Docampo, *Trends in Parasitology*, 19 (2003) 495-501.

8. G. Aguirre, E. Cabrera, H. Cerecetto, R. Di Maio, M. González, G. Seoane, A. Duffaut, A. Denicola, M.J. Gil, V. Martínez-Merino, *European Journal of Medicinal Chemistry*, 39 (2004) 421-431.
9. C. Rigol, C. Olea-Azar, F. Mendizábal, L. Otero, D. Gambino, M. González, H. Cerecetto, *Spectrochimica Acta Part A: Molecular and Biomolecular Spectroscopy*, 61 (2005) 2933-2938.
10. D.H. Geske, J.L. Ragle, M.A. Bambenek, A.L. Balch, *Journal of the American Chemical Society*, 86 (1964) 987-1002.
11. J.H. Freed, G.K. Fraenkel, *The Journal of Chemical Physics*, 39 (1963) 326-348.
12. F.M. Megli, K. Sabatini, *FEBS Letters*, 550 (2003) 185-189.
13. K.K. Mothilal, J. Johnson Inbaraj, R. Gandhidasan, R. Murugesan, *Journal of Photochemistry and Photobiology A: Chemistry*, 162 (2004) 9-16.
14. L. Valgimigli, G.F. Pedulli, M. Paolini, *Free Radical Biology and Medicine*, 31 (2001) 708-716.
15. V.J. Arán, C. Ochoa, L. Boiani, P. Buccino, H. Cerecetto, A. Gerpe, M. González, D. Montero, J.J. Nogal, A. Gómez-Barrio, A. Azqueta, A. López de Ceráin, O.E. Piro, E.E. Castellano, *Bioorganic & Medicinal Chemistry*, 13 (2005) 3197-3207.
16. L. Boiani, A. Gerpe, V.J. Arán, S. Torres de Ortiz, E. Serna, N. Vera de Bilbao, L. Sanabria, G. Yaluff, H. Nakayama, A. Rojas de Arias, J.D. Maya, J.A. Morello, H. Cerecetto, M. González, *European Journal of Medicinal Chemistry*, 44 (2009) 1034-1040.
17. J. Rodríguez, A. Gerpe, G. Aguirre, U. Kemmerling, O.E. Piro, V.J. Arán, J.D. Maya, C. Olea-Azar, M. González, H. Cerecetto, *European Journal of Medicinal Chemistry*, 44 (2009) 1545-1553.
18. J. Rodríguez, C. Olea-Azar, G. Barriga, C. Folch, A. Gerpe, H. Cerecetto, M. González, *Spectrochimica Acta Part A: Molecular and Biomolecular Spectroscopy*, 70 (2008) 557-563.
19. B. Aguilera-Venegas, C. Olea-Azar, E. Norambuena, V.J. Arán, F. Mendizábal, M. Lapier, J.D. Maya, U. Kemmerling, R. López-Muñoz, *Spectrochimica Acta Part A: Molecular and Biomolecular Spectroscopy*, 78 (2011) 1004-1012.
20. J. Dias, A. Silveira, C. Schofield, *Memórias do Instituto Oswaldo Cruz*, 97 (2002) 603-612.
21. J.D. Maya, Y. Repetto, M. Agosin, J.M. Ojeda, R. Tellez, C. Gaule, A. Morello, *Molecular and Biochemical Parasitology*, 86 (1997) 101-106.
22. A.H. Fairlamb, A. Cerami, *Annual Review of Microbiology*, 46 (1992) 695-729.
23. C. Dumas, M. Ouellette, J. Tovar, M.L. Cunningham, A.H. Fairlamb, S. Tamar, M. Olivier, B. Papadopoulou, *EMBO Journal*, 16 (1997) 2590-2598.
24. S. Krieger, W. Schwarz, M.R. Ariyanayagam, A.H. Fairlamb, R.L. Krauth-Siegel, C. Clayton, *Molecular Microbiology*, 35 (2000) 542-552.
25. J. Tovar, M.L. Cunningham, A.C. Smith, S.L. Croft, A.H. Fairlamb, *Proceedings of the National Academy of Sciences of the United States of America*, 95 (1998) 5311-5316.
26. R.L. Krauth-Siegel, M.A. Comini, *Biochimica et Biophysica Acta (BBA) - General Subjects*, 1780 (2008) 1236-1248.
27. A. Saravanamuthu, T.J. Vickers, C.S. Bond, M.R. Peterson, W.N. Hunter, A.H. Fairlamb, *Journal of Biological Chemistry*, 279 (2004) 29493-29500.
28. S.L. Shames, A.H. Fairlamb, A. Cerami, C.T. Walsh, *Biochemistry*, 25 (1986) 3519-3526.
29. A.H. Fairlamb, *Biochemical Society Transactions*, 18 (1990) 717-720.
30. R. Arancibia, A.H. Klahn, G.E. Buono-Core, E. Gutierrez-Puebla, A. Monge, M.E. Medina, C. Olea-Azar, J.D. Maya, F. Godoy, *Journal of Organometallic Chemistry*, 696 (2011) 3238-3244.
31. M. Aravena, R. Figueroa, C. Olea-Azar, V. Aran, *Journal of the Chilean Chemical Society*, 55 (2010) 244-249.
32. C. Folch-Cano, C. Olea-Azar, V.J. Arán, C. Diaz-Urrutia, *Spectrochimica Acta Part A: Molecular and Biomolecular Spectroscopy*, 75 (2010) 375-380.
33. C. Maria Aravena, A. Claudio Olea, H. Cerecetto, M. González, J.D. Maya, J. Rodríguez-Becerra, *Spectrochimica Acta Part A: Molecular and Biomolecular Spectroscopy*, 79 (2011) 312-319.

34. C. Díaz-Urrutia, C. Olea-Azar, G. Zapata, M. Lapier, F. Mura, B. Aguilera-Venegas, V.J. Arán, R. López-Múñoz, J.D. Maya, *Spectrochimica Acta Part A: Molecular and Biomolecular Spectroscopy, in press, corrected proof* (2012).
35. M. Martins Alho, R.N. García-Sánchez, J.J. Nogal-Ruiz, J.A. Escario, A. Gómez-Barrio, A.R. Martínez-Fernández, V.J. Arán, *ChemMedChem*, 4 (2009) 78-87.
36. A. Montero-Torres, R.N. García-Sánchez, Y. Marrero-Ponce, Y. Machado-Tugores, J.J. Nogal-Ruiz, A.R. Martínez-Fernández, V.J. Arán, C. Ochoa, A. Meneses-Marcel, F. Torrens, *European Journal of Medicinal Chemistry*, 41 (2006) 483-493.
37. L.S. Hernández-Muñoz, F.J. González, I. González, M.O.F. Goulart, F.C.d. Abreu, A.S. Ribeiro, R.T. Ribeiro, R.L. Longo, M. Navarro, C. Frontana, *Electrochimica Acta*, 55 (2010) 8325-8335.
38. J.o.P. Telo, A.S. Jalilov, S.F. Nelsen, *The Journal of Physical Chemistry A*, 115 (2011) 3016-3021.
39. J.o.P. Telo, A.l. Moneo, M.F.N.N. Carvalho, S.F. Nelsen, *The Journal of Physical Chemistry A*, 115 (2011) 10738-10743.
40. S.M. Alves Jorge, N.R. Stradiotto, *Journal of Electroanalytical Chemistry*, 431 (1997) 237-241.
41. D.R. Katting, B. Mladenova, G. Grampp, C. Kaiser, A. Heckmann, C. Lambert, *Journal of Physical Chemistry*, 113 (2009) 2983-2995.
42. T.M. Pappenfus, J.D. Raff, E.J. Hukkanen, J.R. Burney, J. Casado, S.M. Drew, L.L. Miller, K.R. Mann, *The Journal of Organic Chemistry*, 67 (2002) 6015-6024.
43. A.J. Bard, L.R. Faulkner, *Wiley, New York*, (1980) 218.
44. A. Rockenbauer, L. Korecz, *Applied Magnetic Resonance*, 10 (1996) 29-43.
45. S. Muelas-Serrano, J.J. Nogal-Ruiz, A. Gómez-Barrio, *Parasitology Research*, 86 (2000) 999-1002.
46. M. Vieites, L. Otero, D. Santos, C. Olea-Azar, E. Norambuena, G. Aguirre, H. Cerecetto, M. González, U. Kemmerling, A. Morello, J. Diego Maya, D. Gambino, *Journal of Inorganic Biochemistry*, 103 (2009) 411-418.
47. M.J.S. Dewar, E.G. Zoebisch, E.F. Healy, J.J.P. Stewart, *Journal of the American Chemical Society*, 107 (1985) 3902-3909.
48. A.R. Katritzky, M. Szafran, E. Anders, N. Malhotra, S.U. Chaudry, *Tetrahedron Computer Methodology*, 3 (1990) 247-269.
49. E. Klein, M. Matis, V. Lukes, Z. Cibulková, *Polymer Degradation and Stability*, 91 (2006) 262-270.
50. Y. Sun, D. Chen, C. Liu, *Journal of Molecular Structure: THEOCHEM*, 618 (2002) 181-189.
51. M. D'Amore, R. Improta, V. Barone, *Journal of Physical Chemistry A*, 107 (2003) 6264-6269.
52. G.W.T. M. J. Frisch, H. B. Schlegel, G. E. Scuseria, J.R.C. M. A. Robb, G. Scalmani, V. Barone, B. Mennucci, H.N. G. A. Petersson, M. Caricato, X. Li, H. P. Hratchian, J.B. A. F. Izmaylov, G. Zheng, J. L. Sonnenberg, M. Hada, K.T. M. Ehara, R. Fukuda, J. Hasegawa, M. Ishida, T. Nakajima, O.K. Y. Honda, H. Nakai, T. Vreven, J. A. Montgomery, Jr., F.O. J. E. Peralta, M. Bearpark, J. J. Heyd, E. Brothers, V.N.S. K. N. Kudin, R. Kobayashi, J. Normand, A.R. K. Raghavachari, J. C. Burant, S. S. Iyengar, J. Tomasi, N.R. M. Cossi, J. M. Millam, M. Klene, J. E. Knox, J. B. Cross, C.A. V. Bakken, J. Jaramillo, R. Gomperts, R. E. Stratmann, A.J.A. O. Yazyev, R. Cammi, C. Pomelli, J. W. Ochterski, K.M. R. L. Martin, V. G. Zakrzewski, G. A. Voth, J.J.D. P. Salvador, S. Dapprich, A. D. Daniels, J.B.F. O. Farkas, J. V. Ortiz, J. Cioslowski, G. and D. J. Fox, Inc., Wallingford CT, *Gaussian09.*, 2009.
53. A.D. Becke, *Physical Review A*, 38 (1988) 3098-3100.
54. C.T. Lee, W.T. Yang, R.G. Parr, *Physical Review B*, 37 (1988) 785-789.
55. V. Barone, M. Cossi, *Journal of Physical Chemistry A*, 102 (1998) 1995-2001.
56. M. Cossi, V. Barone, R. Cammi, J. Tomasi, *Chemical Physics Letters*, 255 (1996) 327-335.
57. [57] S.I. Gorelsky, A.B.P. Lever, *Journal of Organometallic Chemistry*, 635 (2001) 187-196.
58. S.I. Gorelsky, University of Ottawa, http://www.sg-chem.net/, (2010).

59. N.M. O'Boyle, A.L. Tenderholt, K.M. Langner, *Journal of Computational Chemistry*, 29 (2008) 839-845.
60. Garrett M. Morris, David S. Goodsell, Robert S. Halliday, Ruth Huey, William E. Hart, Richard K. Belew, Arthur J. Olson, *Journal of Computational Chemistry*, 19 (1998) 1639-1662.
61. Y. Zhang, C.S. Bond, S. Bailey, M.L. Cunningham, A.H. Fairlamb, W.N. Hunter, *Protein Science*, 5 (1996) 52-61.
62. T.J. Dolinsky, P. Czodrowski, H. Li, J.E. Nielsen, J.H. Jensen, G. Klebe, N.A. Baker, *Nucleic Acids Research*, 35 (2007) W522-W525.
63. T.J. Dolinsky, J.E. Nielsen, J.A. McCammon, N.A. Baker, *Nucleic Acids Research*, 32 (2004) W665-W667.
64. N.A. Macias-Ruvalcaba, J.P. Telo, D.H. Evans, *Journal of Electroanalytical Chemistry*, 600 (2007) 294-302.
65. J.A. Bautista-Martínez, I. González, M. Aguilar-Martínez, *Electrochimica Acta*, 49 (2004) 3403-3411.
66. S. Bollo, L.J. Núñez-Vergara, M. Bontá, G. Chauviere, J. Périé, J.A. Squella, *Journal of Electroanalytical Chemistry*, 511 (2001) 46-54.
67. J. Carbajo, S. Bollo, L.J. Núñez-Vergara, A. Campero, J.A. Squella, *Journal of Electroanalytical Chemistry*, 531 (2002) 187-194.
68. R.S. Nicholson, I. Shain, *Analytical Chemistry*, 36 (1964) 706-723.
69. M.L. Olmstead, R.G. Hamilton, R.S. Nicholson, *Analytical Chemistry*, 41 (1969) 260-267.
70. M.L. Olmstead, R.S. Nicholson, *Analytical Chemistry*, 41 (1969) 862-864.
71. L. Nadjo, J.M. Saveant, *Journal of Electroanalytical Chemistry and Interfacial Electrochemistry*, 33 (1971) 419-451.
72. G.P. Mamatha, B.S. Sherigara, K.M. Mahadevan, *Indian Journal of Chemical Technology*, 14 (2007) 556-571.
73. M.B. Robin, P. Day, Mixed Valence Chemistry-A Survey and Classification, H.J. Emeléus, A.G. Sharpe (Eds.) *Advances in Inorganic Chemistry*, Volume 10, Academic Press, 1968, pp. 247-422.
74. C.S. Johnson, *Molecular Physics: An International Journal at the Interface Between Chemistry and Physics*, 12 (1967) 25-31.
75. V. Barone, *Chemical Physics Letters*, 262 (1996) 201-206.
76. D. Vujosevic, R. Scheuermann, H. Dilger, I.M. Tucker, A. Martyniak, I. McKenzie, E. Roduner, *Physica B: Condensed Matter*, 374-375 (2006) 295-298.
77. X. Xu, Q. Zhang, R.P. Muller, W.A.G. III, *The Journal of Chemical Physics*, 122 (2005) 014105.
78. C. Alemán, M.C. Vega, J.J. Perez, *Journal of Molecular Structure: THEOCHEM*, 281 (1993) 39-44.
79. M.T. Nguyen, S. Creve, L.G. Vanquickenborne, *The Journal of Physical Chemistry A*, 101 (1997) 3174-3181.
80. V. Barone, *World Scientific Publishing*, (1995).
81. N. Rega, M. Cossi, V. Barone, *The Journal of Chemical Physics*, 105 (1996) 11060-11067.
82. R.G. Parr, L.v. Szentpály, S. Liu, *Journal of the American Chemical Society*, 121 (1999) 1922-1924.
83. A.H. Fairlamb, *Transactions of the Royal Society of Tropical Medicine and Hygiene*, 84 (1990) 613-617.
84. C. Olea-Azar, H. Cerecetto, A. Gerpe, M. González, V.J. Arán, C. Rigol, L. Opazo, *Spectrochimica Acta Part A: Molecular and Biomolecular Spectroscopy*, 63 (2006) 36-42.
85. C. Olea-Azar, C. Rigol, F. Mendizábal, R. Briones, H. Cerecetto, R. Di Maio, M. Risso, M. González, W. Porcal, *Spectrochimica Acta Part A: Molecular and Biomolecular Spectroscopy*, 59 (2003) 69-74.
86. R.L. Krauth-Siegel, G.H. Coombs, *Parasitology Today*, 15 (1999) 404-409.

87. A. Gerpe, G. Aguirre, L. Boiani, H. Cerecetto, M. González, C. Olea-Azar, C. Rigol, J.D. Maya, A. Morello, O.E. Piro, V.J. Arán, A. Azqueta, A.L. de Ceráin, A. Monge, M.A. Rojas, G. Yaluff, *Bioorganic & Medicinal Chemistry*, 14 (2006) 3467-3480.
88. C. Viodé, N. Bettache, N. Cenas, R.L. Krauth-Siegel, G. Chauvière, N. Bakalara, J. Périé, *Biochemical Pharmacology*, 57 (1999) 549-557.
89. E. Finkelstein, G.M. Rosen, E.J. Rauckman, J. Paxton, *Molecular Pharmacology*, 16 (1979) 676-685.
90. A. Lawrence, C.M. Jones, P. Wardman, M.J. Burkitt, *Journal of Biological Chemistry*, 278 (2003) 29410-29419.